Role of Hall effect on resistive kink mode in Tokamak

W. Zhang, Z. W. Ma[a)], H. W. Zhang, and X. Wang
Institute for Fusion Theory and Simulation, Department of Physics, Zhejiang University, Hangzhou 310027, China

Abstract: The influence of the Hall effect on the nonlinear evolution of the m/n=1/1 resistive-kink mode is numerically investigated by the three-dimensional toroidal Hall-MHD code CLT. It is found that the Hall effect can lead to the explosive growth of the resistive-kink mode at the nonlinear stage. The explosive nonlinear growth of the resistive-kink mode mainly results from the structural transition of the current sheet in the Hall-MHD simulations. At the nonlinear stage, the geometry of the current sheet turns into X-type from Y-type, resulting in the significant acceleration of the reconnection process. The fast reconnection induced by the Hall effect may explain the fast crash observed in large Tokamaks. We also found that there exists a critical value of the ion inertial length that is resulted from the acceleration of magnetic reconnection due to the decoupling motions of ions and electrons and the suppression effect by the electron diamagnetic rotation in the Hall MHD. The critical value of d_i decreases with increasing thermal conductivity $\kappa_\perp$. When d_i exceeds a critical value, the peak growth rate decreases with increasing d_i.

a) Email address: zwma@zju.edu.cn

I. Introduction

Sawtooth in magnetically confined fusion devices (such as Tokamaks) is periodic oscillations of the core temperature with a rapid drop (about 10-100 μs) after a slow rise (about a few milliseconds).[1-3] Sawtooth is one of the most common phenomena in Tokamaks when the safety factor on the magnetic axis is below 1.0. Sawtooth plays an important role in Tokamak performance because it can trigger neo-classical tearing mode instabilities[4, 5] on other rational surfaces, which are very deleterious for plasma confinement. It can also influence the confinement of α particles.[6] Therefore, for magnetically confined fusion reactors, it is crucial to understand the physical mechanism behind sawtooth oscillations.

Sawtooth was firstly observed in 1974 in the symmetric Tokamak.[1] Kadomtsev[7] then proposed a complete reconnection model to explain the temperature crash in the core region with the crash time $\tau_c \sim (\tau_A \tau_R)^{1/2}$, where τ_A and τ_R are the Alfvén and resistive diffusion times, respectively. However, as plasmas become hotter in large Tokamaks (such as JET[8] and TFTR[9]), the resistivity of plasmas in these experiments becomes lower. Therefore, the crash time predicted in the Kadomtsev's model is about two orders of magnitude larger than the observed crash times. In order to resolve this big difference, many works on sawtooth [4, 10-40] have been carried out.

Aydemir[15] firstly found that the *m/n*=1/1 resistive kink mode exhibits a nonlinearly enhanced growth rate that far exceeds its linear growth rate due to collisionless modification in the four-field model given by Hazeltine et al. [41]. Shortly after that, Wang and Bhattacharjee[16] presented an analytical theory for the nonlinear dynamical evolution of the *m/n*=1/1 resistive kink mode, governed by the Hall term. It successfully explains the nonlinearly enhanced growth rates -the acceleration of reconnection results from the geometry transition in the reconnection diffusion region. In the framework of resistive-MHD, which does not include Hall terms, the current sheet becomes thinner and elongated. Therefore, the geometry of the current sheet is Y-type during the nonlinear evolution of the resistive-kink mode. The Y-type current sheet implies that the time scale of magnetic reconnection will be slow [42]. However, in the framework of Hall-MHD, the current sheet shrinks and becomes in the same order of the current thickness. Thus, the current sheet in the diffusion region has an X-type geometry. Such geometry transition in the nonlinear stage results in the fast reconnection process [43-45]. However, these studies are either based on the reduced MHD model in the cylindrical geometry or carried out with compressible Hall MHD model in the slab geometry, and a toroidal investigation is then needed to ensure that the fast crash observed in Tokamaks is indeed related to Hall effects. However, three-dimensional (3D) Hall MHD simulations in the toroidal geometry are not easy to be conducted. The difficulty of a 3D Hall MHD simulation is that the Hall term can introduce a dispersive dispersion relation $\omega \sim k^2$ that causes severe problems on the numerical stability.[43, 44] Recently, Beidler et al. firstly presented 3D toroidal Hall-MHD simulations on the fast reconnection during the sawtooth crash through an implicit code M3D-C1.[20] In the present paper, we will carry out our 3D toroidal Hall-MHD simulations by an explicit code.

II. The Hall-MHD Model in CLT

The CLT code is a three-dimensional toroidal Hall-MHD code. The 4th order finite difference method in the R, ϕ, and Z directions, and the 4th order Runge–Kutta scheme in the time integration are applied.[45] The full set of the Hall-MHD equations used in the CLT code is given as follows:

$$\frac{\partial \rho}{\partial t} = -\nabla \cdot (\rho \mathbf{v}) + \nabla \cdot [D\nabla(\rho\text{-}\rho_0)], \tag{1}$$

$$\frac{\partial p}{\partial t} = -\mathbf{v} \cdot \rlap{\boldsymbol{\kappa}}\nabla p - \Gamma p \nabla \cdot \mathbf{v} + \nabla \cdot [\quad \nabla(p - p_0)], \tag{2}$$

$$\frac{\partial \mathbf{v}}{\partial t} = -\mathbf{v} \cdot \nabla \mathbf{v} + (\mathbf{J} \times \mathbf{B} - \nabla p) / \rho + \nabla \cdot [\upsilon \nabla (\mathbf{v} - \mathbf{v}_0)], \tag{3}$$

$$\frac{\partial \mathbf{B}}{\partial t} = -\nabla \times \mathbf{E}, \tag{4}$$

$$\mathbf{E} = -\mathbf{v} \times \mathbf{B} + \eta(\mathbf{J} - \mathbf{J}_0) + \frac{d_i}{\rho}(\mathbf{J} \times \mathbf{B} - \nabla p), \tag{5}$$

$$\mathbf{J} = \frac{1}{\mu_0}\nabla\times\mathbf{B}, \tag{6}$$

where ρ, p, p_e, $\mathbf{v}$, $\mathbf{B}$, $\mathbf{E}$, and $\mathbf{J}$ are the mass density, the total plasma pressure, the electron pressure, the plasma velocity, the magnetic field, the electric field, and the current density, respectively. The plasma pressure is contributed only from electrons due to the assumption of cold ions, i.e., $p = p_e$. The subscript "0" means the initial value. $\Gamma(=5/3)$ is the ratio of specific heat of plasma. The normalization of the variables used in the present paper are: $\mathbf{B}/B_{00}\to\mathbf{B}$, $\mathbf{x}/a\to\mathbf{x}$, $\rho/\rho_{00}\to\rho$, $\mathbf{v}/v_A\to\mathbf{v}$, $t/t_A\to t$, $p/(B_{00}^2/\mu_0)\to p$, $\mathbf{J}/(B_{00}/\mu_0 a)\to\mathbf{J}$, and $\mathbf{E}/(v_A B_{00})\to\mathbf{E}$, where a is the minor radius, $v_A = B_{00}/\sqrt{\mu_0\rho_{00}}$ is the Alfvén speed, and $t_A = a/v_A$ is the Alfvén time. B_{00} and ρ_{00} are the initial magnetic field and mass density at the magnetic axis, respectively. $d_i = c/\omega_{pi}$ is the ion inertial length, where ω_{pi} is the ion plasma frequency. η, D, $\kappa_\perp$, $\kappa_\parallel$, and υ are the resistivity, the plasma diffusion coefficient, the perpendicular and parallel thermal conductivity, and the viscosity, respectively, and normalized as follows: $\eta/(\mu_0 a^2/t_A)\to\eta$, $D/(a^2/t_A)\to D$, $\kappa_\perp/(a^2/t_A)\to\kappa_\perp$, $\kappa_\parallel/(a^2/t_A)\to\kappa_\parallel$, and $\upsilon/(a^2/t_A)\to\upsilon$.

III. Simulation results

A. Fast reconnection induced by Hall effect

A toroidal Tokamak geometry with a circular cross-section is chosen in our simulations (the major radius $R_0 = 4$ and the minor radius $a = 1$). The initial safety factor and pressure profiles are shown in Figure 1. Since the safety factor at the magnetic axis is $q_0 = 0.7$, the most unstable mode in the system is the m/n=1/1 resistive kink mode. The equilibrium is obtained from the NOVA code.[46] The benchmarking could be seen from our previous studies.[47] The grids used in the present paper are $400\times64\times400$ (R,ϕ,Z). Since there are 64 grids in the ϕ direction, the maximum toroidal mode number is 32. The convergence studies have been ensured by using different grids, i. e. $256\times64\times256$, $400\times64\times400$, and $400\times128\times400$ (R,ϕ,Z), respectively. In the present paper, the resistivity, the viscosity, the plasma diffusivity, the parallel and perpendicular thermal conductivity, are chosen to be $\eta=3\times10^{-6}$, $\upsilon=3\times10^{-5}$, $D=1.0\times10^{-4}$, $\kappa_{\parallel}=5\times10^{-2}$, and $\kappa_{\perp}=3.0\times10^{-5}$ to $\kappa_{\perp}=3.0\times10^{-7}$, respectively. The resistivity in the present paper is constant and remains unchanged during the simulation.

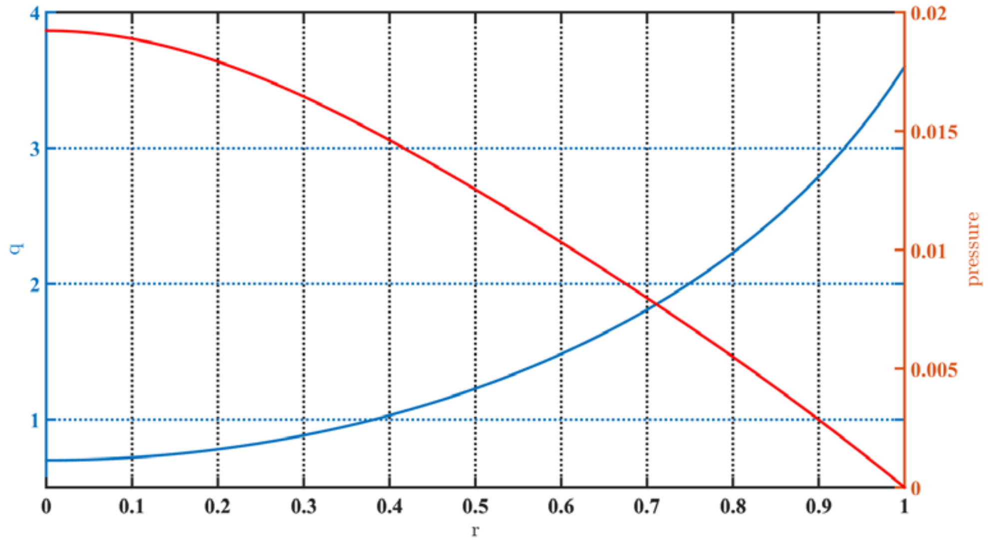

Figure 1. The initial q and pressure profiles. $r=\sqrt{\psi_{norm}}$, where ψ_{norm} is the normalized magnetic flux.

In this subsection, we conduct two typical cases with $d_i=0$ (resistive-MHD) and $d_i=0.15$ (Hall-MHD) to illustrate influences of the Hall effect on the nonlinear evolution of the *m/n*=1/1 resistive-kink mode. The evolutions of the kinetic energy and the growth rate for the *m/n*=1/1 resistive-kink mode with and without the Hall effect are shown in Figure 2. The linear growth rates for the two cases are both about 0.006. In the nonlinear stage, the growth rates of the kinetic energy in both cases exhibit enhancement. In the resistive case, the enhancement of the nonlinear growth rate is associated with that magnetic reconnection is accelerated by the external inward flow[48] induced by internal kink instability. In the Hall case, the burst in the nonlinear phase results from both external inward flow and the Hall effects[49]. Hall terms can lead to the separated motion of ions and electrons in the vicinity of the diffusion region with the spatial scale d_i. The influence of the Hall effect can be dominant when the current sheet is sufficiently thin. As a result, the elongated thin current sheet shrinks, and the reconnection rate exhibits a significant enhancement. The maximum growth rate for the case with $d_i = 0.15$ is about 0.026, which is four times larger than its linear growth rate. These results agree well with previous cylindrical simulations[15] and theoretical analysis.[16]

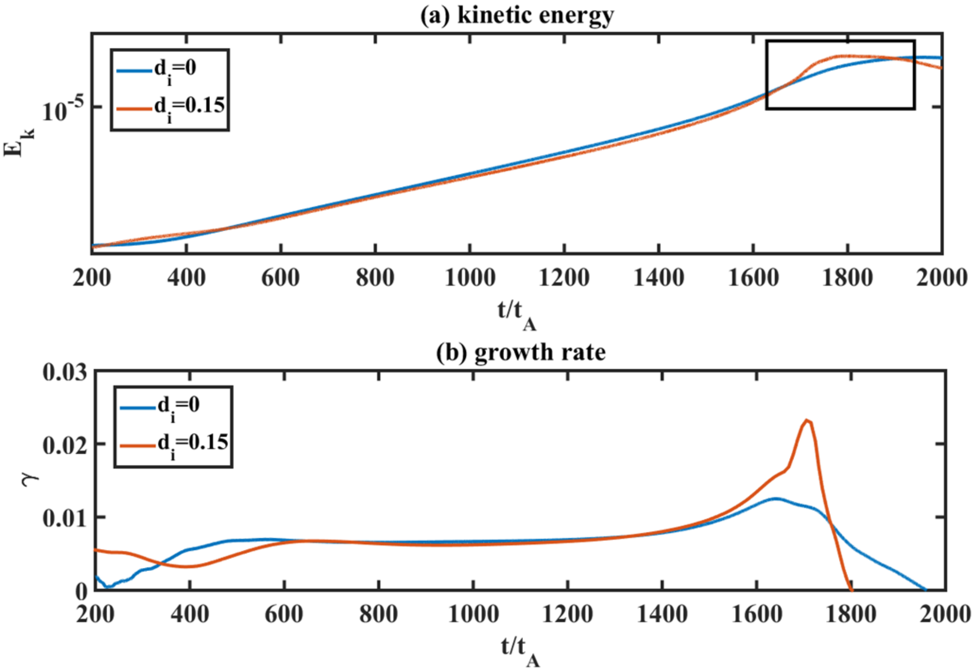

Figure 2 The evolutions of (a) the kinetic energy and (b) the growth rate for the m/n=1/1 resistive-kink mode with and without the Hall effect. The growth rate is defined as $\gamma = \partial(\ln E_k)/\partial t$, and is normalized with t_A^{-1}, where t_A is the Alfven time. The kinetic energy is normalized with $\rho_0 V_A^2$.

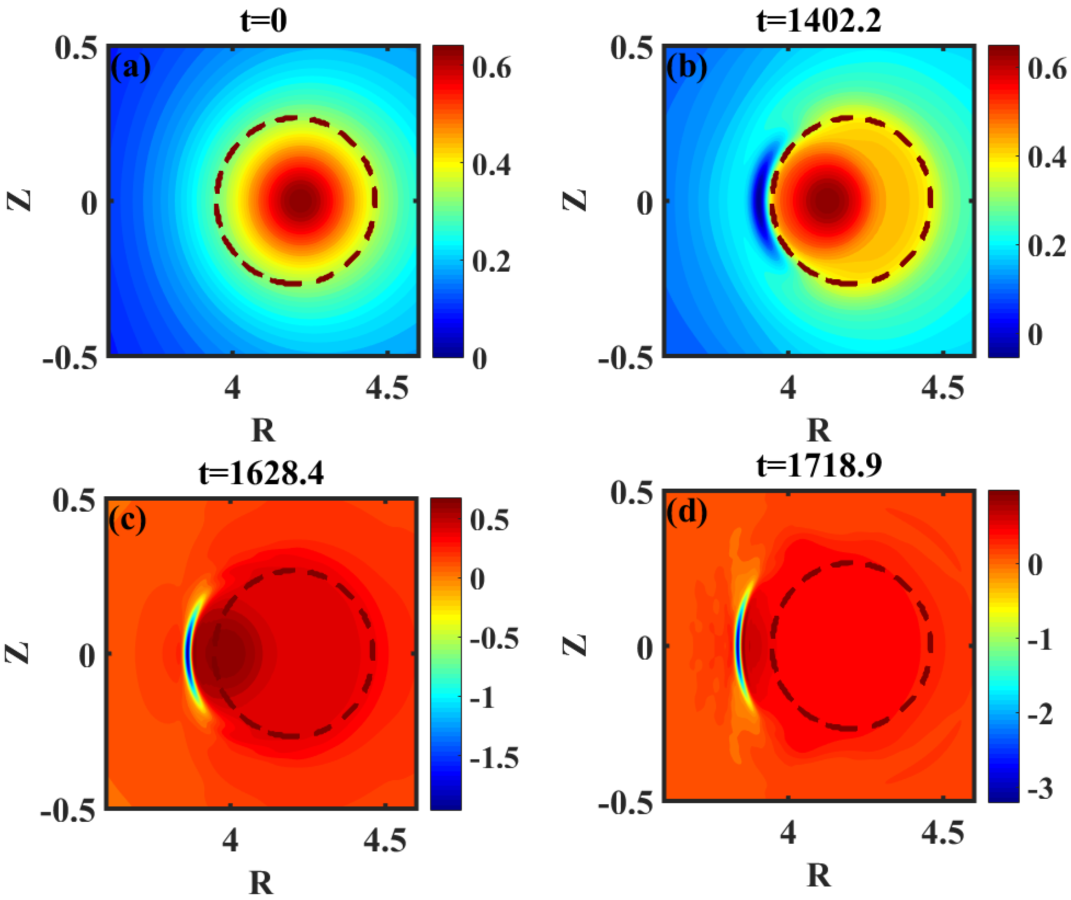

Figure 3. The snapshots of the contour plots of the toroidal current density in the resistive-MHD simulation in the poloidal plane with $\phi = 0$ at (a) $t = 0t_A$, (b) $t = 1402.2t_A$, (c) $t = 1628.4t_A$, and (d) $t = 1718.9t_A$. The dark red dashed line is the initial q=1 surface.

Figure 3 shows the snapshots of the toroidal current density in the resistive-MHD simulation. It indicates that the reconnection in the diffusion region keeps Sweet-Parker[42] (or called Y-type) reconnection throughout the evolution of the resistive-kink mode. The current sheet is thin and strong at the nonlinear stage, as shown in Figure 3(d). It could also be seen from the Poincare plots of the magnetic field (Figure 4). With the Hall effect, the current sheet structure at the linear and early nonlinear stage is similar to that in resistive-MHD simulation, as shown in Figure 5 (a) and (b). However, when the thickness of the current sheet reduces to a critical value, the Hall terms start to play a dominant role during the reconnection. Then the elongated thin current sheet shrinks, and the current sheet geometry in the diffusion region turns into the X-type from the Y-type (Figure 5 c and d). Since the X-type reconnection could be much faster than the Y-type reconnection, the kinetic energy experiences explosive growth, and the maximum reconnection rate in the nonlinear stage becomes much larger than that in the linear stage.

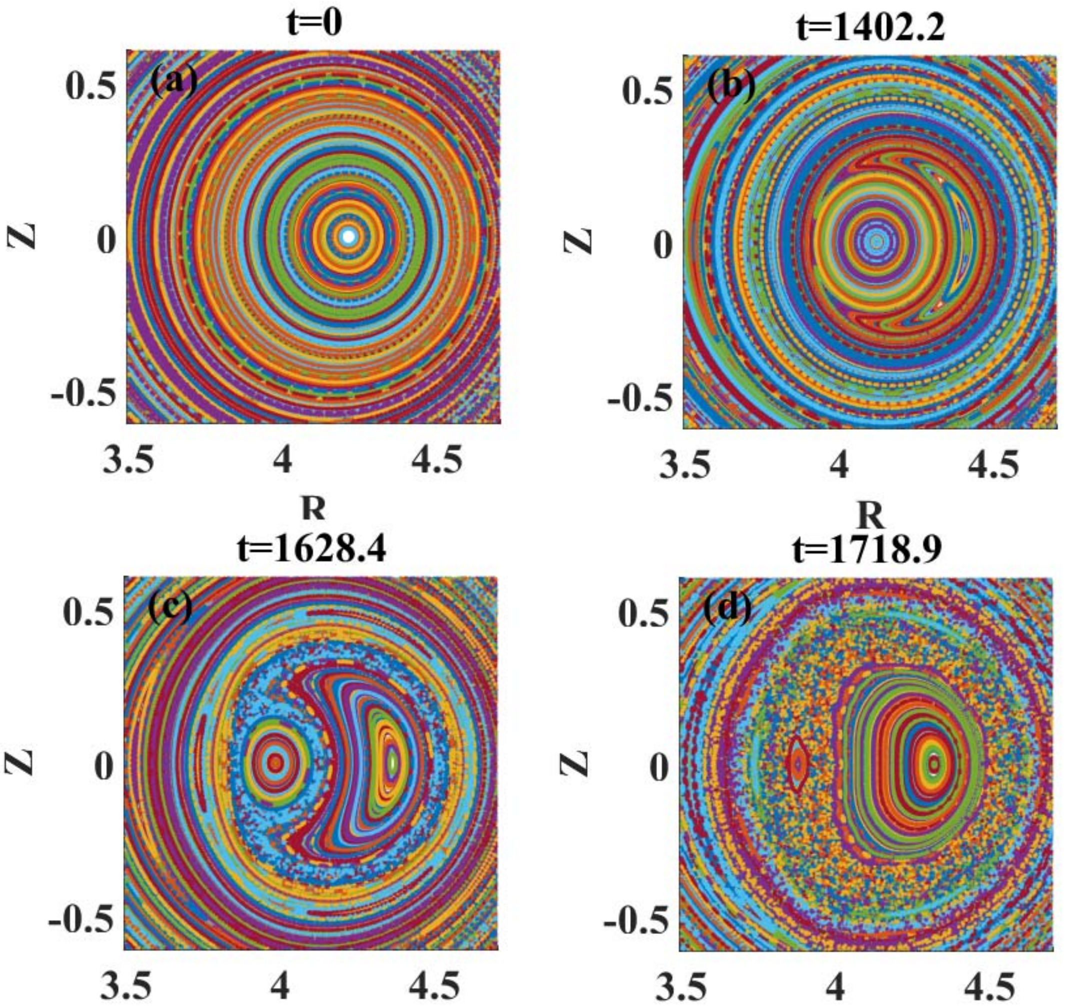

Figure 4 The Poincaré plots of the magnetic field in the Hall-MHD simulation in the poloidal plane with $\phi = 0$ at (a) $t = 0t_A$, (b) $t = 1402.2t_A$, (c) $t = 1628.4t_A$, and (d) $t = 1718.9t_A$.

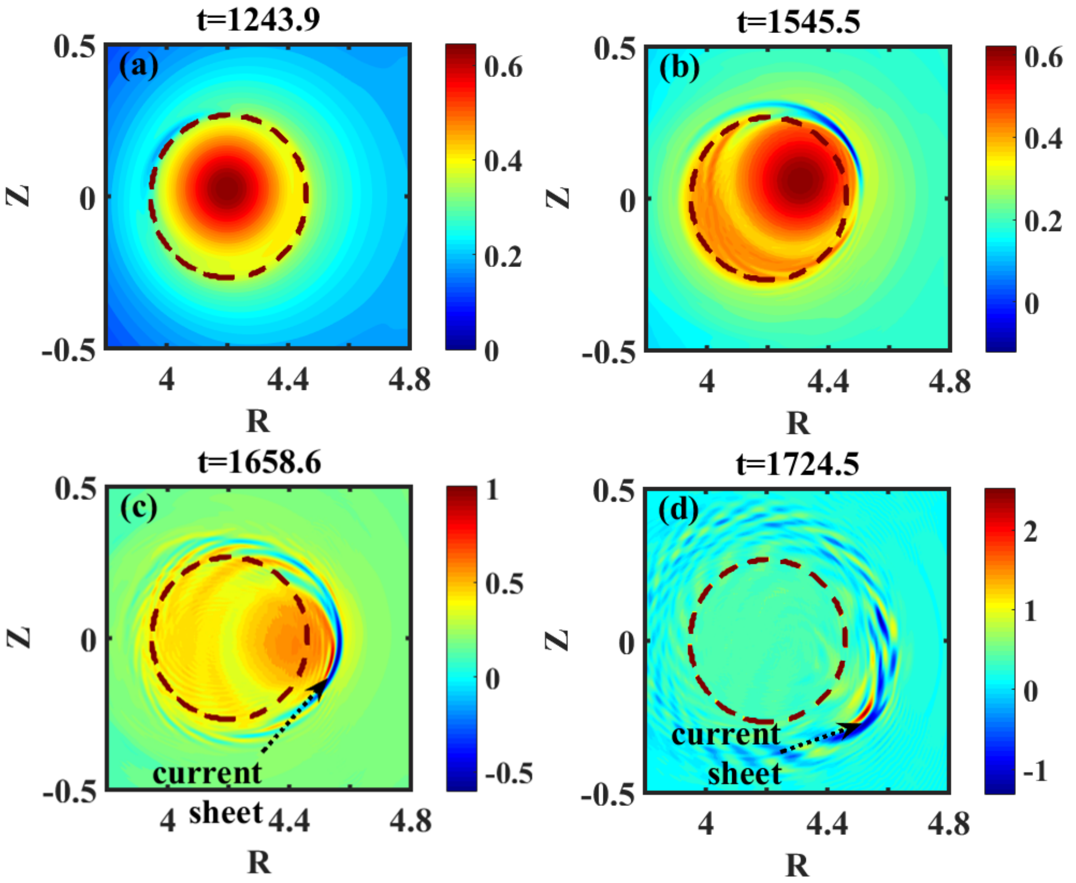

Figure 5. The snapshots of the contour plots of the toroidal current density in the Hall-MHD simulation in the poloidal plane with $\phi = 0$ at (a) $t = 1243.9 t_A$, (b) $t = 1545.5 t_A$, (c) $t = 1658.6 t_A$, and (d) $t = 1724.5 t_A$. The dark red dashed line is the initial q=1 surface.

The evolution of the growth rate for the resistive-MHD and Hall-MHD simulations are shown in Figure 6 (a) and (b). At the linear stage, other modes($n \neq 1$) are resulted from the beats of the $n = 1$ mode for both resistive-MHD simulations and Hall-MHD simulations, since their growth rates are approximately equal to multiple times of the growth rate of $n = 1$ mode. However, the behavior of the beat modes could be extremely different at the nonlinear stage. For the resistive-MHD simulations, the nonlinear growth rates of the high n modes decrease. However, in the Hall-MHD simulations, the growth rates of the high n modes significantly increase at the nonlinear stage, which suggests that the explosive growth at the nonlinear stage is mainly due to the fast development of the high n modes.

(a) resistive-MHD

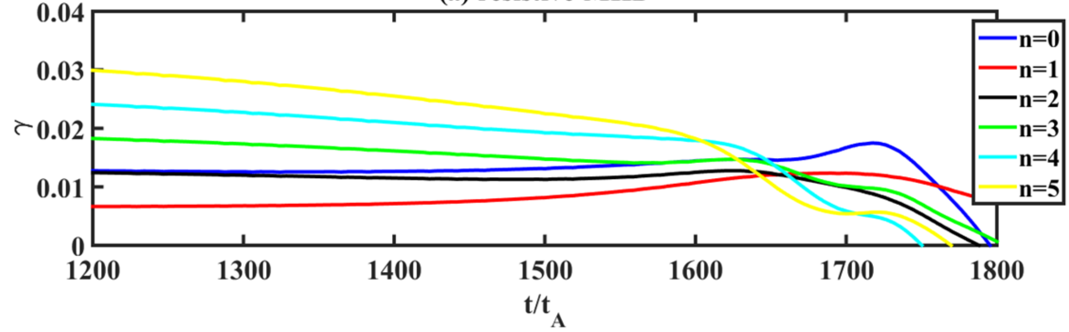

(b) Hall-MHD

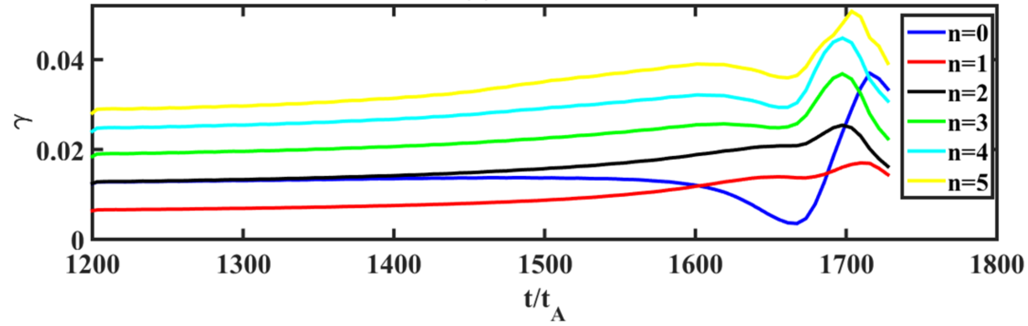

Figure 6 The evolution of the growth rate for modes with different toroidal numbers (a) the resistive-MHD and (b) the Hall-MHD simulations.

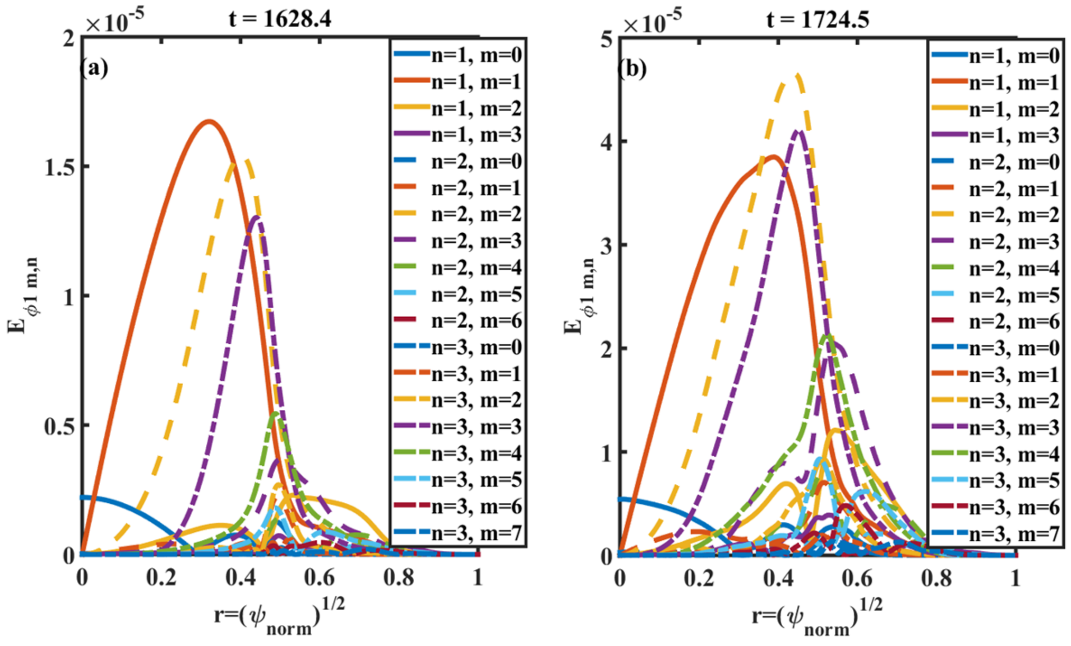

Figure 7 The mode structures of the resistive-kink mode at the time with the maximum growth rate for (a) resistive-MHD and (b) Hall-MHD.

The mode structures of the resistive-kink mode at the time with the maximum growth rate for (a) resistive-MHD and (b) Hall-MHD are shown in Figure 7. The harmonics of the *m/n*=1/1 mode are also well developed at the nonlinear stage. In the framework of resistive-MHD, the amplitudes of the *m/n*=2/2 and 3/3 modes are lower than that of the *m/n*=1/1 component. However, in the Hall-MHD simulations, the amplitudes of the *m/n*=2/2 and 3/3 modes become larger than that of the *m/n*=1/1 component. The energy spectrums are shown in Figure 8 (a) resistive-MHD and (b) Hall-MHD, which also indicates that the *m/n*=1/1 mode and its harmonics are the dominant modes in the system, and strong harmonics of the *m/n*=1/1 mode appear in Hall-MHD simulations.

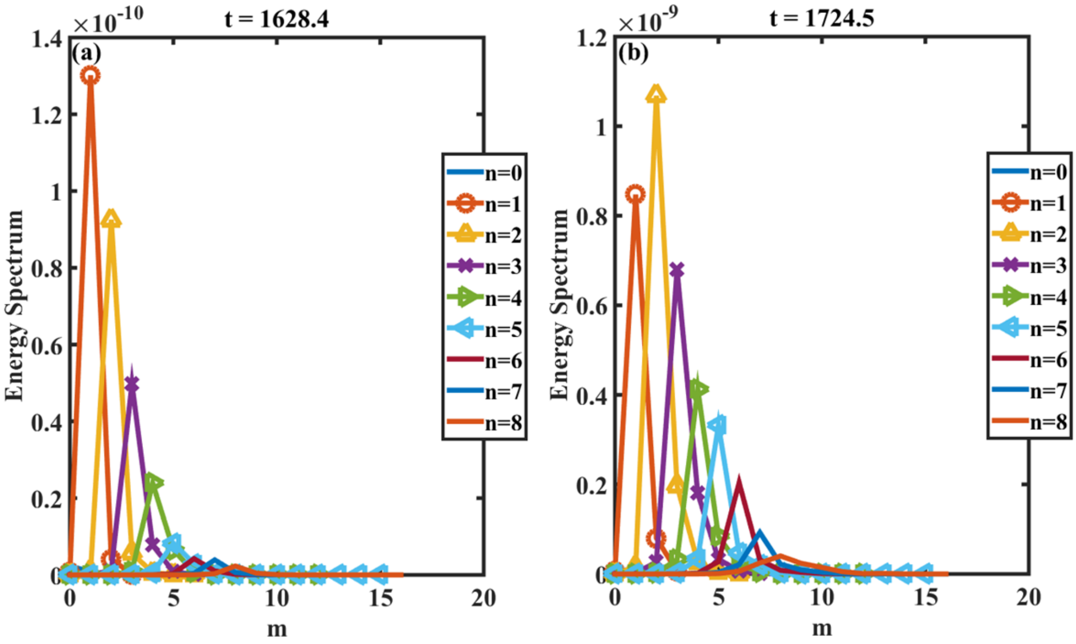

Figure 8 The energy spectrum of the resistive-kink mode at the time with the maximum growth rate for (a) resistive-MHD and (b) Hall-MHD.

It should be noted that the current sheet rotates in the clockwise direction with $d_i = 0.15$ (Figure 5), which means that the resistive-kink mode has a real frequency in Hall-MHD simulations. The mode rotation could also be seen from the Poincaré plots of the magnetic field (Figure 9). However, the real frequency is zero in resistive-MHD simulations (Figure 3 and 4). The real frequency of the resistive-kink mode results from the electron diamagnetic drift introduced by Hall terms. Since the electron diamagnetic drift frequency $\omega_{*e} = -\frac{m}{n_0 e r B_T} \frac{dp_e}{dr}$ is proportional to the poloidal mode number m, the harmonics of the *m/n*=1/1 mode have different rotation frequency. That is the reason why there exists some ‘ripple’ on the contour plot of toroidal current at the nonlinear stage (Figure 5. b and c).

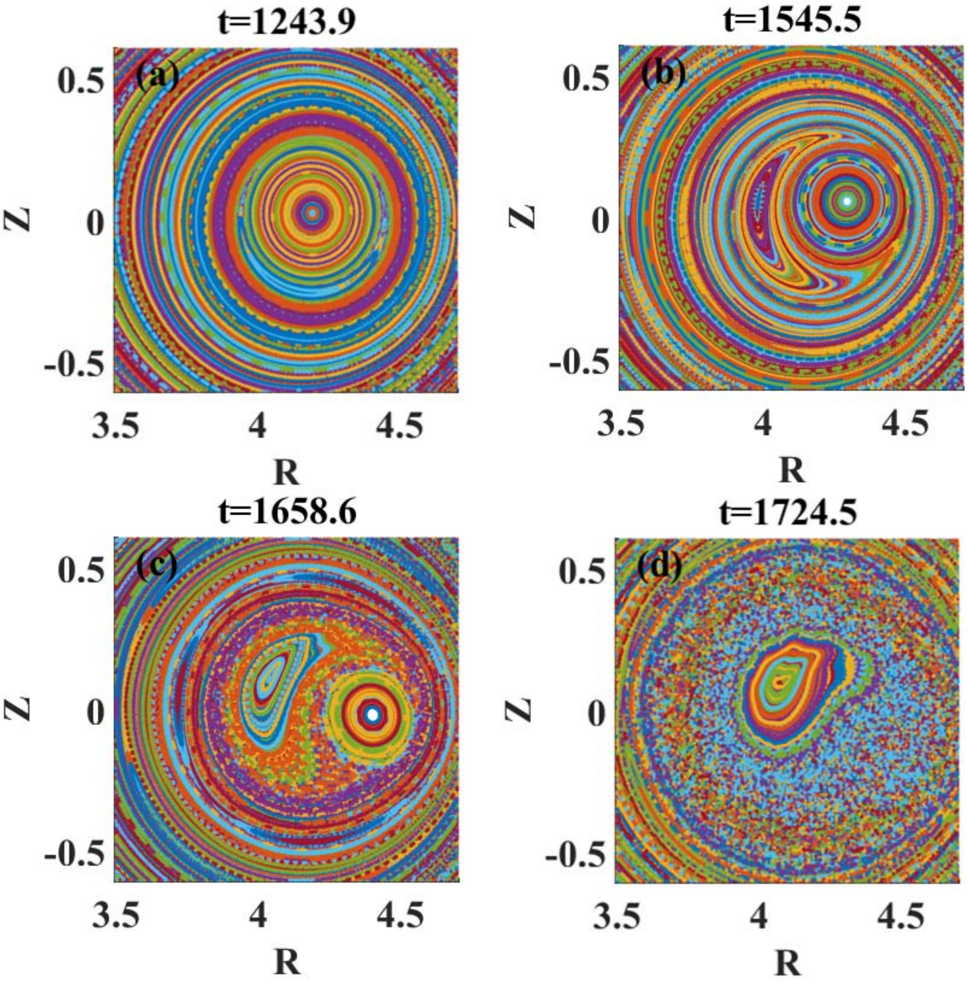

Figure 9. The Poincaré plots of the magnetic field in the Hall-MHD simulation in the poloidal plane with $\phi = 0$ at (a) $t = 1243.9t_A$, (b) $t = 1545.5t_A$, (c) $t = 1658.6t_A$, and (d) $t = 1724.5t_A$.

The contour images of the pressure and the safety factor q at the nonlinear stage in the Hall-MHD simulations are shown in Figure 10. At $t = 1658.6t_A$, the safety factor at the magnetic axis is about 0.7 that is the same with the initial value as shown in Figure 10c. After the reconnection, the minimum q in the whole region becomes 1.0 (Figure 10 d), which indicates that it is a complete reconnection. At $t = 1724.5t_A$, the original core is squeezed to the X-point and almost disappears. As a result, a peak of pressure profiles forms near X-point (Figure 10 b), and the plasma pressure becomes almost flattened in other regions. However, due to the stochasticity of the magnetic field in the broad region, the original core could not be clearly seen from the Poincare plots (Figure 9 d) or the safety factor image (Figure 10 d). The stochasticity of the magnetic field mainly results from the development of different helical modes.

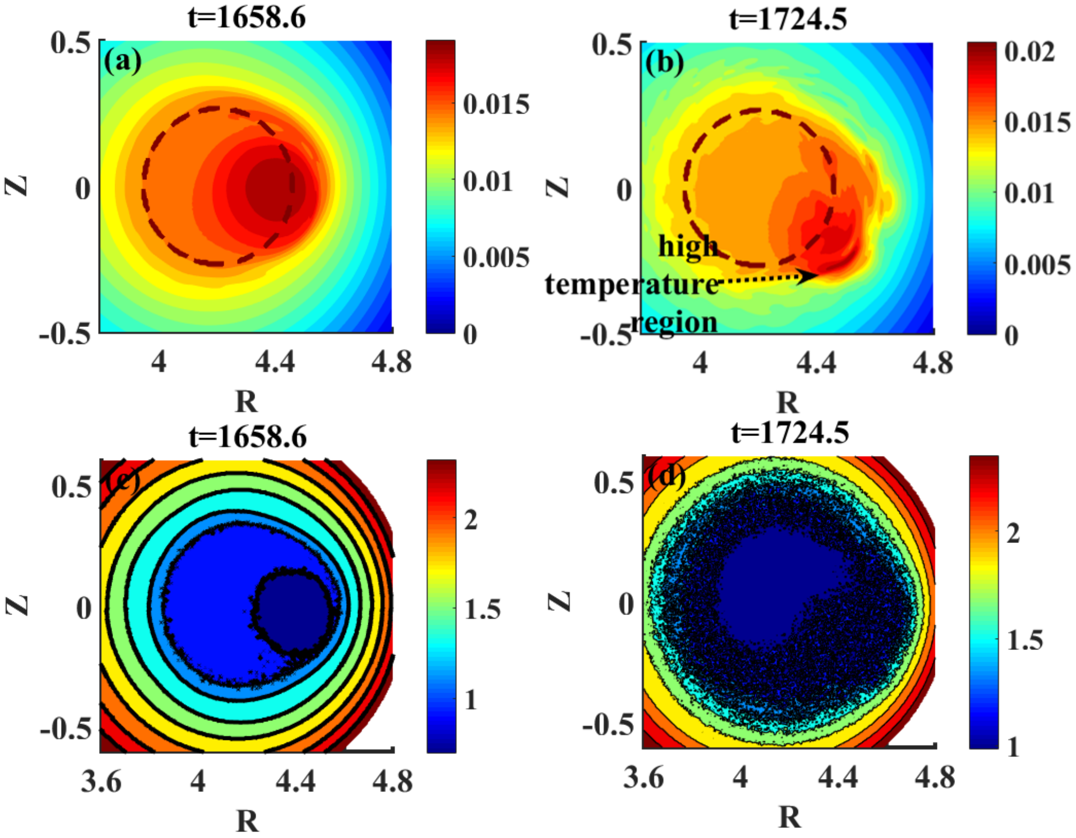

Figure 10 The contour plot of the total plasma pressure at (a) $t = 1658.6t_A$, and (b) $t = 1724.5t_A$ in the poloidal plane with $\phi = 0$. The dark red dashed line is the initial q=1 surface. The contour plot of safety factor profiles in the poloidal plane with $\phi = 0$ at (c) $t = 1658.6t_A$, and (d) $t = 1724.5t_A$.

B. The nonlinear evolution of the resistive-kink mode with different d_i

The inclusion of Hall terms in the generalized Ohm's law leads to two effects: the electron diamagnetic drift,[53] which could reduce the growth rate of the resistive-kink mode, and the structural transition of the thin current sheet, [16]which could significantly enhance the nonlinear reconnection rate. For typical parameters in the present Tokamaks, the particle density is about $n = 2 \sim 4\times10^{19} m^{-3}$, the ion plasma frequency is about $\omega_{pi} = 0.6 \sim 0.8\times10^{10} s^{-1}$, the minor radius is $a \sim 0.5$ and $c = 3\times10^{8} m/s$, then we have $d_i = c/\omega_{pi} = 4 \sim 5$cm and $d_i / a \sim 0.1$. As a result, the range of the ion inertial length in the present subsection is scanned from $d_i = 0$ to $d_i = 0.2$. The linear growth rates of the resistive-kink mode with different $\kappa_\perp$ and d_i are shown in Figure 11, which is similar to our previous studies.[50]

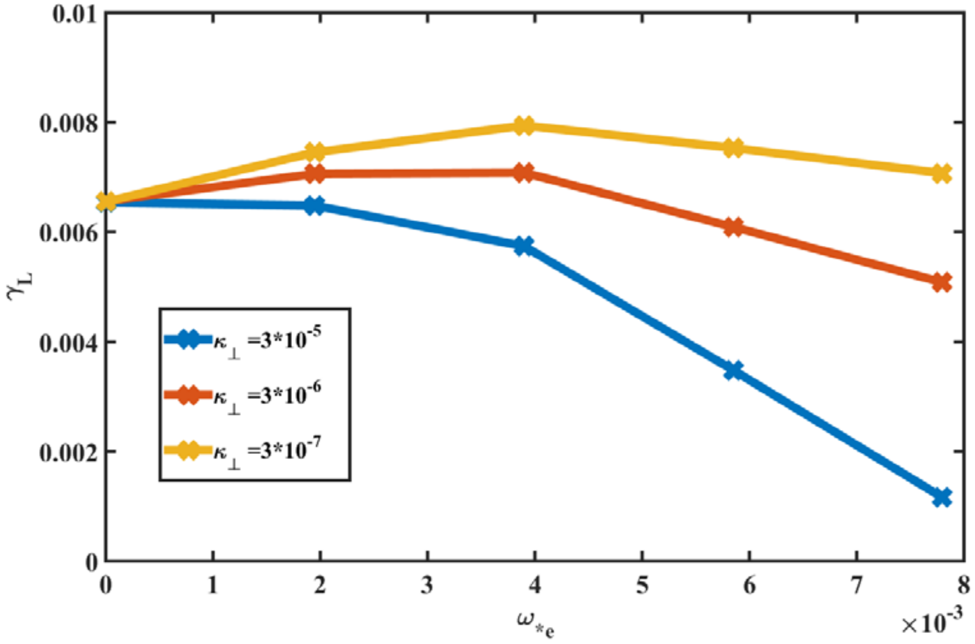

Figure 11 The linear growth rates of the resistive-kink mode with different $\kappa_\perp$ and d_i.

The evolutions of the growth rates with $\kappa_\perp = 3\times10^{-6}$ and different d_i are shown in Figure 12. It is found that there exists a critical value ($d_i \sim 0.12$). For the cases with $d_i < 0.12$, the maximum nonlinear growth rate increases with increasing d_i. However, for the cases with $d_i > 0.12$, the maximum nonlinear growth rate decreases with increasing d_i.

It should be noted that the electron diamagnetic drift velocity is proportional to d_i, and it can significantly suppress the resistive-kink mode when the perpendicular thermal conductivity is large while the electron magnetic drift only has little influence on the growth rate of the resistive-kink mode when $\kappa_\perp$ is small. It implies that the critical value of d_i is due to the competition between the suppression by the electron diamagnetic rotation and the acceleration of magnetic reconnection by decoupling motions of ions and electrons in the Hall MHD.

As indicated in Figure 11, the electron magnetic drift only has little influence on the growth rate of the resistive-kink mode with a small thermal conductivity. Therefore, we further conduct the cases with $\kappa_\perp = 3\times10^{-7}$ and different d_i to show the acceleration of magnetic reconnection by the Hall effect. From Figure 13, the maximum growth rate in the case with $d_i = 0.2$ is about 0.029, which is only slightly smaller than that with $d_i = 0.15$ (the maximum growth rate is about 0.031). When $\kappa_\perp = 3\times10^{-5}$, the maximum growth rate with $d_i = 0.15$ is even smaller than that in the resistive-MHD simulation (Figure 14). With $d_i = 0.2$, the linear growth rate of the resistive-kink mode further decreases to 0.001, which means that the mode is almost fully suppressed by the electron diamagnetic drift. The simulation results for the cases with $\kappa_\perp = 3\times10^{-7}$ and $\kappa_\perp = 3\times10^{-5}$ in Figure 13 and Figure 14 suggest that as d_i increases, the decrease of the maximum nonlinear growth rate is mainly due to the increase of the electron diamagnetic rotation.

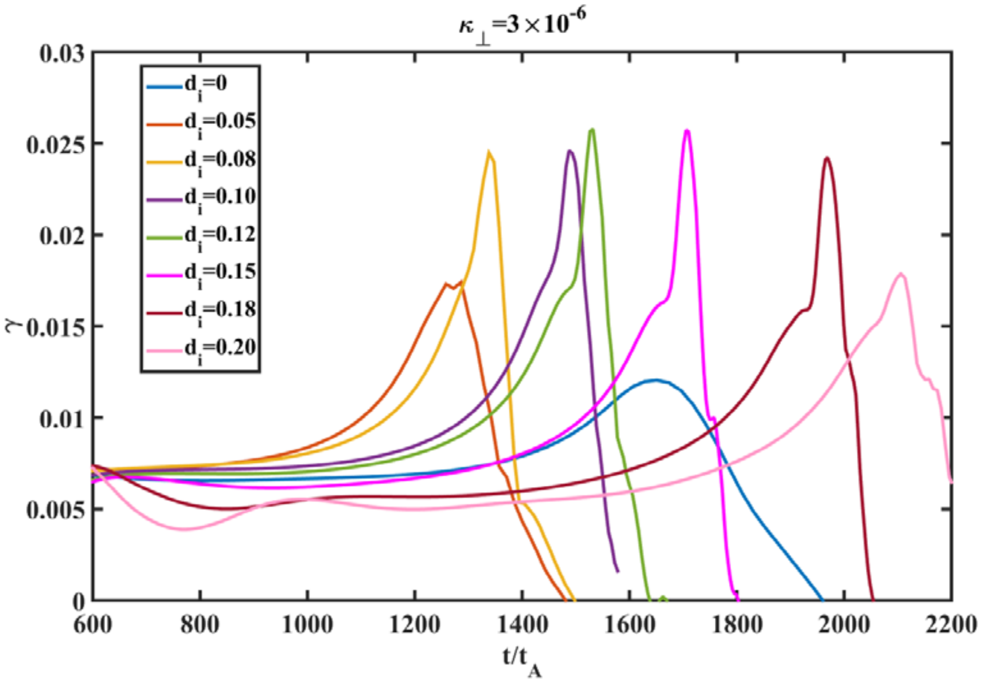

Figure 12 The evolutions of the growth rates with $\kappa_\perp = 3\times10^{-6}$ and different d_i.

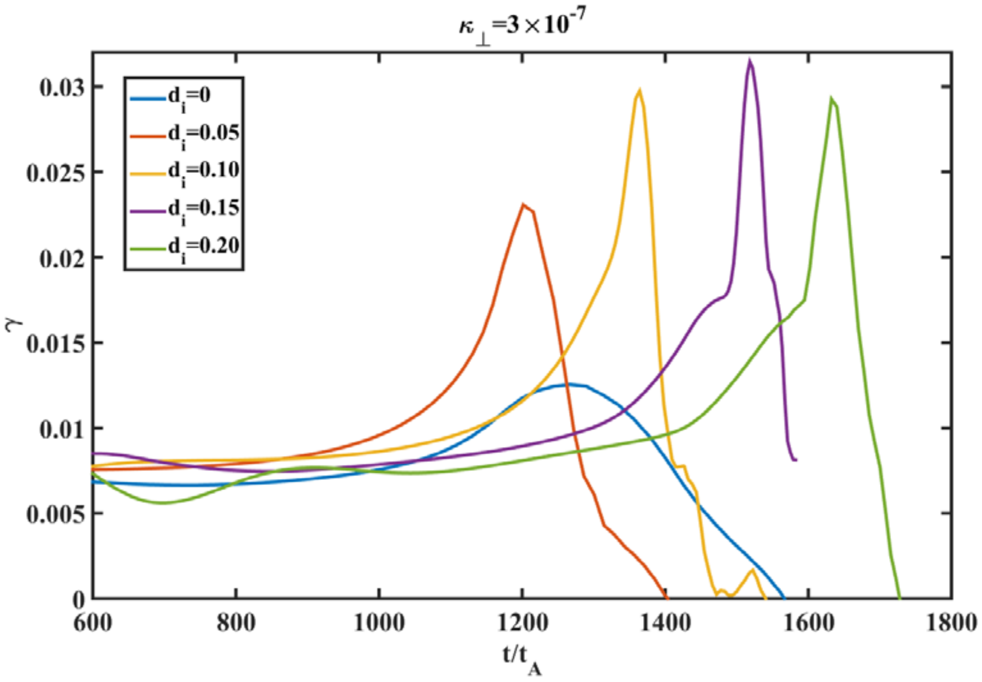

Figure 13 The evolutions of the growth rates with $\kappa_\perp = 3\times10^{-7}$ and different d_i.

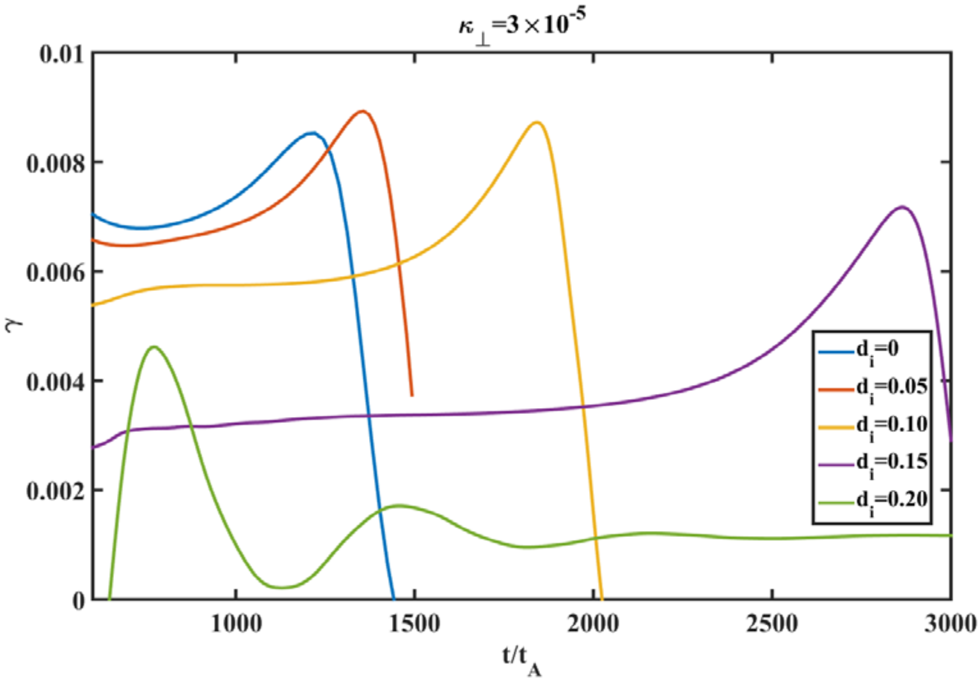

Figure 14 The evolutions of the growth rates with $\kappa_\perp = 3\times10^{-5}$ and different d_i.

A series of numerical simulations with the application of GPU acceleration [45] is carried out to study the nonlinear dynamics of the resistive kink mode under different ion inertial length and the perpendicular thermal conductivities. It is found that the Hall effect can lead to the explosive growth of the resistive-kink mode at the nonlinear stage, which agrees well with previous theoretical predictions[16] and simulation results.[20, 38] The acceleration of reconnection results from the geometry transition in the reconnection diffusion region. In the framework of resistive-MHD, the current sheet becomes thinner and elongated. The geometry of the current sheet remains Y-type during the nonlinear evolution of the resistive-kink mode. However, in the framework of Hall-MHD, the length of the current sheet shrinks, and the geometry of the diffusion region changes from Y-type to X-type at the nonlinear stage, resulting in a fast reconnection process. It is also found that the increase of the ion inertial length (d_i) does not always lead to an increase of the nonlinear growth rate. When d_i is smaller than the critical value, the maximum growth rate increases with increasing d_i; however, when d_i is larger than the critical value, the maximum growth rate decreases with increasing d_i. It is due to competition between the suppression by the electron diamagnetic drift and the acceleration by the Hall effect. Besides, the perpendicular thermal conductivity $\kappa_\perp$ is also found to have a significant influence on the maximum growth rate and the critical value of d_i, which both decrease with increasing $\kappa_\perp$.

IV. SUMMARY

The influence of the Hall effect on the nonlinear evolution of the $m/n=1/1$ resistive-kink mode is investigated. It is found that the Hall effect can lead to the explosive growth of the resistive-kink mode at the nonlinear stage, which is consistent with earlier theoretical predictions.[16] The explosive nonlinear growth mainly results from the structural transition of the current sheet. In the framework of resistive-MHD, the current sheet remains in a Y-type geometry in the entire simulation period. However, the current sheet turns into X-type at the nonlinear stage from Y-type at the linear stage in the Hall-MHD simulation, resulting in the significant acceleration of the reconnection process. The nonlinear explosive growth of the $m/n=1/1$ resistive-kink mode can be the right candidate to explain the fast pressure crash observed in large Tokamaks.[8, 9]

It should be noted that the maximum nonlinear growth rate does not always increase with increasing ion inertial length (d_i). There exists a critical value. If d_i is smaller than the critical value, the maximum growth rate increases with increasing d_i; if d_i exceeds the critical value, the maximum growth rate decreases with increasing d_i. It results from the competition between the acceleration of magnetic reconnection due to the decoupling motions of ions and electrons and the suppression by the electron diamagnetic rotation in the Hall MHD. The critical value of d_i decreases with increasing the thermal conductivity $\kappa_\perp$. For $\kappa_\perp = 3\times10^{-6}$, the critical value of the ion inertial length is $d_i = 0.12$. It also should be noted that the maximum growth rate also strongly depends on the perpendicular thermal conductivity.

Acknowledgment

This work is supported by the National Natural Science Foundation of China under Grant No. 11775188 and 11835010, the Special Project on High-performance Computing under the National Key R&D Program of China No. 2016YFB0200603, Fundamental Research Fund for Chinese Central Universities.

Reference

[1] S. von Goeler, W. Stodiek, N. Sauthoff, Studies of Internal Disruptions and $m=1$ Oscillations in Tokamak Discharges with Soft\char22{}X-Ray Tecniques, Physical Review Letters, 33 (1974) 1201-1203.

[2] K. McGuire, D.C. Robinson, Sawtooth oscillations in a small tokamak, Nuclear Fusion, 19 (1979) 505.

[3] M.A. Dubois, A.L. Pecquet, C. Reverdin, Internal disruptions in the TFR tokamak: A phenomenological analysis, Nuclear Fusion, 23 (1983) 147.

[4] V. Igochine, A. Gude, S. Günter, K. Lackner, Q. Yu, L.B. Orte, A. Bogomolov, I. Classen, R.M. McDermott, N.C.L. Jr., A.U. Team, Conversion of the dominantly ideal perturbations into a tearing mode after a sawtooth crash, Physics of Plasmas, 21 (2014) 110702.

[5] R.J. Buttery, T.C. Hender, D.F. Howell, R.J.L. Haye, O. Sauter, D. Testa, Onset of neoclassical tearing modes on JET, Nuclear Fusion, 43 (2003) 69.

[6] I.T. Chapman, Controlling sawtooth oscillations in tokamak plasmas, Plasma Physics and Controlled Fusion, 53 (2011) 013001.

[7] B. Kadomtsev, Disruptive instability in Tokamaks(helical plasma motions), Soviet Journal of Plasma Physics, 1 (1975) 389-391.

[8] A.W. Edwards, D.J. Campbell, W.W. Engelhardt, H.U. Fahrbach, R.D. Gill, R.S. Granetz, S. Tsuji, B.J.D. Tubbing, A. Weller, J. Wesson, D. Zasche, Rapid Collapse of a Plasma Sawtooth Oscillation in the JET Tokamak, Physical Review Letters, 57 (1986) 210-213.

[9] K. McGuire, V. Arunasalam, C.W. Barnes, M.G. Bell, M. Bitter, R. Boivin, N.L. Bretz, R. Budny, C.E. Bush, A. Cavallo, T.K. Chu, S.A. Cohen, P. Colestock, S.L. Davis, D.L. Dimock, H.F. Dylla, P.C. Efthimion, A.B. Ehrhrardt, R.J. Fonck, E. Fredrickson, H.P. Furth, G. Gammel, R.J. Goldston, G. Greene, B. Grek, L.R. Grisham, G. Hammett, R.J. Hawryluk, H.W. Hendel, K.W. Hill, E. Hinnov, D.J. Hoffman, J. Hosea, R.B. Howell, H. Hsuan, R.A. Hulse, A.C. Janos, D. Jassby, F. Jobes, D.W. Johnson, L.C. Johnson, R. Kaita, C. Kieras‐Phillips, S.J. Kilpatrick, P.H. LaMarche, B. LeBlanc, D.M. Manos, D.K. Mansfield, E. Mazzucato, M.P. McCarthy, M.C. McCune, D.H. McNeill, D.M. Meade, S.S. Medley, D.R. Mikkelsen, D. Monticello, R. Motley, D. Mueller, J.A. Murphy, Y. Nagayama, D.R. Nazakian, E.B. Neischmidt, D.K. Owens, H. Park, W. Park, S. Pitcher, A.T. Ramsey, M.H. Redi, A.L. Roquemore, P.H. Rutherford, G. Schilling, J. Schivell, G.L. Schmidt, S.D. Scott, J.C. Sinnis, J. Stevens, B.C. Stratton, W. Stodiek, E.J. Synakowski, W.M. Tang, G. Taylor, J.R. Timberlake, H.H. Towner, M. Ulrickson, S.v. Goeler, R. Wieland, M. Williams, J.R. Wilson, K.L.

Wong, M. Yamada, S. Yoshikawa, K.M. Young, M.C. Zarnstorff, S.J. Zweben, High ‑ beta operation and magnetohydrodynamic activity on the TFTR tokamak, Physics of Fluids B: Plasma Physics, 2 (1990) 1287-1290.

[10] J.A. Wesson, Sawtooth oscillations, Plasma Physics and Controlled Fusion, 28 (1986) 243.

[11] Y.I. Kolesnichenko, Y.V. Yakovenko, D. Anderson, M. Lisak, F. Wising, Sawtooth oscillations with the central safety factor, ${\mathit{q}}_{0}$, below unity, Physical Review Letters, 68 (1992) 3881-3884.

[12] I.T. Chapman, R. Scannell, W.A. Cooper, J.P. Graves, R.J. Hastie, G. Naylor, A. Zocco, Magnetic Reconnection Triggering Magnetohydrodynamic Instabilities during a Sawtooth Crash in a Tokamak Plasma, Physical Review Letters, 105 (2010) 255002.

[13] A.J. Lichtenberg, K. Itoh, S.I. Itoh, A. Fukuyama, The role of stochasticity in sawtooth oscillations, Nuclear Fusion, 32 (1992) 495.

[14] F. Porcelli, D. Boucher, M.N. Rosenbluth, Model for the sawtooth period and amplitude, Plasma Physics and Controlled Fusion, 38 (1996) 2163.

[15] A.Y. Aydemir, Nonlinear studies of m=1 modes in high ‑ temperature plasmas, Physics of Fluids B: Plasma Physics, 4 (1992) 3469-3472.

[16] X. Wang, A. Bhattacharjee, Nonlinear dynamics of the m=1 instability and fast sawtooth collapse in high-temperature plasmas, Physical Review Letters, 70 (1993) 1627-1630.

[17] S. Günter, Q. Yu, K. Lackner, A. Bhattacharjee, Y.M. Huang, Fast sawtooth reconnection at realistic Lundquist numbers, Plasma Physics and Controlled Fusion, 57 (2015) 014017.

[18] J.A. Breslau, S.C. Jardin, W. Park, Three-dimensional modeling of the sawtooth instability in a small tokamak, Physics of Plasmas, 14 (2007) 056105.

[19] M.T. Beidler, P.A. Cassak, Model for Incomplete Reconnection in Sawtooth Crashes, Physical Review Letters, 107 (2011) 255002.

[20] M.T. Beidler, P.A. Cassak, S.C. Jardin, N.M. Ferraro, Local properties of magnetic reconnection in nonlinear resistive- and extended-magnetohydrodynamic toroidal simulations of the sawtooth crash, Plasma Physics and Controlled Fusion, 59 (2017) 025007.

[21] F.D. Halpern, D. Leblond, H. Lütjens, J.F. Luciani, Oscillation regimes of the internal kink mode in tokamak plasmas, Plasma Physics and Controlled Fusion, 53 (2010) 015011.

[22] F.D. Halpern, H. Lütjens, J.-F. Luciani, Diamagnetic thresholds for sawtooth cycling in tokamak plasmas, Physics of Plasmas, 18 (2011) 102501.

[23] R. Fischer, A. Bock, A. Burckhart, O.P. Ford, L. Giannone, V. Igochine, M. Weiland, M. Willensdorfer, Sawtooth induced q-profile evolution at ASDEX Upgrade, Nuclear Fusion, 59 (2019) 056010.

[24] I. Krebs, S.C. Jardin, S. Günter, K. Lackner, M. Hoelzl, E. Strumberger, N. Ferraro, Magnetic flux pumping in 3D nonlinear magnetohydrodynamic simulations, Physics of Plasmas, 24 (2017) 102511.

[25] M.I. Mironov, F.S. Zaitsev, N.N. Gorelenkov, V.I. Afanasyev, F.V. Chernyshev, V.G. Nesenevich, M.P. Petrov, Sawtooth mixing of alphas, knock-on D, and T ions, and its influence on NPA spectra in ITAB, Nuclear Fusion, 58 (2018) 082030.

[26] W. Guo, J. Wang, D. Liu, X. Wang, A resistive magnetodynamics analysis of sawtooth driven tearing modes in tokamak plasmas, Physics of Plasmas, 23 (2016) 062117.

[27] S.C. Jardin, N. Ferraro, I. Krebs, Self-Organized Stationary States of Tokamaks, Physical Review Letters, 115 (2015) 215001.

[28] Y.B. Nam, J.S. Ko, G.H. Choe, Y. Bae, M.J. Choi, W. Lee, G.S. Yun, S. Jardin, H.K. Park, Validation of the 'full reconnection model' of the sawtooth instability in KSTAR, Nuclear Fusion, 58 (2018) 066009.

[29] G. Kim, G.S. Yun, M. Woo, Mitigation of sawtooth crash as a manifestation of MHD mode coupling

prior to disruption of KSTAR plasma, Plasma Physics and Controlled Fusion, 61 (2019) 055001.

[30] E. Li, V. Igochine, O. Dumbrajs, L. Xu, K. Chen, T. Shi, L. Hu, The non-resonant kink modes triggering strong sawtooth-like crashes in the EAST tokamak, Plasma Physics and Controlled Fusion, 56 (2014) 125016.

[31] G.S. Li, T. Zhang, M.F. Wu, H.M. Xiang, Y.M. Wang, F. Wen, Y. Liu, K.N. Geng, F.B. Zhong, K.X. Ye, Y. Sun, J. Huang, H.Q. Liu, S.B. Zhang, X.D. Lin, X. Gao, Destabilization of field-line localized density fluctuation with a 1/1 internal kink mode in the EAST tokamak, Nuclear Fusion, 59 (2019) 096032.

[32] A.Y. Aydemir, J.Y. Kim, B.H. Park, J. Seol, On resistive magnetohydrodynamic studies of sawtooth oscillations in tokamaks, Physics of Plasmas, 22 (2015) 032304.

[33] M. Jiang, Y. Xu, W. Chen, Z.B. Shi, J.Q. Li, W.X. Wang, Z.H. Qin, X.T. Ding, W.L. Zhong, X.Q. Ji, P.W. Shi, Z.C. Yang, B.S. Yuan, Y. Liu, Q.W. Yang, M. Xu, Localized modulation of turbulence by m/n = 1/1 magnetic islands in the HL-2A tokamak, Nuclear Fusion, 59 (2019) 066019.

[34] A. Ali, P. Zhu, Effects of plasmoid formation on sawtooth process in a tokamak, Physics of Plasmas, 26 (2019) 052518.

[35] D. Liu, W.W. Heidbrink, M. Podestà, G.Z. Hao, D.S. Darrow, E.D. Fredrickson, D. Kim, Effect of sawtooth crashes on fast ion distribution in NSTX-U, Nuclear Fusion, 58 (2018) 082028.

[36] G.H. Choe, G.S. Yun, H.K. Park, J.H. Jeong, Slow crash in modified sawtooth patterns driven by localized electron cyclotron heating and current drive in KSTAR, Nuclear Fusion, 58 (2018) 106038.

[37] J.-H. Ahn, X. Garbet, H. Lütjens, A. Marx, T. Nicolas, R. Sabot, J.-F. Luciani, R. Guirlet, O. Février, P. Maget, Non-linear dynamics of compound sawteeth in tokamaks, Physics of Plasmas, 23 (2016) 052509.

[38] Q. Yu, S. Günter, K. Lackner, Numerical modelling of sawtooth crash using two-fluid equations, Nuclear Fusion, 55 (2015) 113008.

[39] D. Brunetti, J.P. Graves, F.D. Halpern, J.F. Luciani, H. Lütjens, W.A. Cooper, Extended MHD simulations of infernal mode dynamics and coupling to tearing modes, Plasma Physics and Controlled Fusion, 57 (2015) 054002.

[40] A. Kleiner, J.P. Graves, D. Brunetti, W.A. Cooper, F.D. Halpern, J.F. Luciani, H. Lütjens, Neoclassical tearing mode seeding by coupling with infernal modes in low-shear tokamaks, Nuclear Fusion, 56 (2016) 092007.

[41] R.D. Hazeltine, C.T. Hsu, P.J. Morrison, Hamiltonian four‐field model for nonlinear tokamak dynamics, The Physics of Fluids, 30 (1987) 3204-3211.

[42] E.N. Parker, Sweet's mechanism for merging magnetic fields in conducting fluids, Journal of Geophysical Research, 62 (1957) 509-520.

[43] S.C. Jardin, Review of implicit methods for the magnetohydrodynamic description of magnetically confined plasmas, Journal of Computational Physics, 231 (2012) 822-838.

[44] W. Park, E.V. Belova, G.Y. Fu, X.Z. Tang, H.R. Strauss, L.E. Sugiyama, Plasma simulation studies using multilevel physics models, Physics of Plasmas, 6 (1999) 1796-1803.

[45] H. Zhang, J. Zhu, Z. Ma, G. Kan, X. Wang, W. Zhang, Acceleration of three-dimensional Tokamak magnetohydrodynamical code with graphics processing unit and OpenACC heterogeneous parallel programming, International Journal of Computational Fluid Dynamics, (2019) 1-14.

[46] C. Cheng, M. Chance, NOVA: A nonvariational code for solving the MHD stability of axisymmetric toroidal plasmas, Journal of Computational Physics, 71 (1987) 124-146.

[47] S. Wang, Z. Ma, Influence of toroidal rotation on resistive tearing modes in tokamaks, Physics of Plasmas, 22 (2015) 122504.

[48] X.G. Wang, A. Bhattacharjee, Z.W. Ma, Scaling of collisionless forced reconnection, Physical review letters, 87 (2001) 265003.

[49] X.G. Wang, A. Bhattacharjee, Z.W. Ma, Collisionless reconnection: Effects of Hall current and electron pressure gradient, Journal of Geophysical Research: Space Physics, 105 (2000) 27633-27648.

[50] W. Zhang, Z.W. Ma, H.W. Zhang, J. Zhu, Dynamic evolution of resistive kink mode with electron diamagnetic drift in tokamaks, Physics of Plasmas, 26 (2019) 042514.